Evanescent-field-induced second harmonic generation by noncentrosymmetric nanoparticles

Ronja Bäumner[1], Luigi Bonacina[2,*], Jörg Enderlein[3], Jérôme Extermann[2], Thomas Fricke-Begemann[1], Gerd Marowsky[1], Jean-Pierre Wolf[2]

[1] *Laser Laboratorium Göttingen e.V., Hans-Adolf Krebsweg 1, 37077 Göttingen, Germany*
[2] *Université de Genève, GAP-Biophotonics, 20 Rue de l'Ecole de Médecine, 1211 Geneva 4, Switzerland*
[3] *III. Institute of Physics, Georg August University, 37077 Göttingen, Germany*
luigi.bonacina@unige.ch

Abstract: We demonstrate the excitation of second harmonic radiation of noncentrosymmetric nanoparticles dispersed on a planar optical waveguide by the evanescent field of the guided mode. Polarization imaging reveals information on the orientation of the crystal axis of individual nanoparticles. Interference patterns generated from adjacent particles at the second harmonic frequency are - to the authors knowledge - observed for the first time. The actual form of the interference pattern is explained on the basis of a dipole radiation model, taking into account the nanoparticles' orientation, surface effects, and the characteristics of the imaging optics.

OCIS codes: 230.7370 Waveguides; 190.2620 Harmonic generation and mixing; 310.6628 Subwavelength structures, nanostructures

References and links

1. G. L. Duveneck, M. Pawlak, D. Neuschafer, E. Bar, W. Budach, and U. Pieles, "Novel bioaffinity sensors for trace analysis based on luminescence excitation by planar waveguides," Sens. Actuators B **38**, 88–95 (1997).
2. P. N. Zeller, G. Voirin, and R. E. Kunz, "Single-pad scheme for integrated optical fluorescence sensing," Biosens. Bioelectron. **15**, 591–595 (2000).
3. K. Schmitt, K. Oehse, G. Sulz, and C. Hoffmann, "Evanescent field sensors based on tantalum pentoxide waveguides - a review," Sensors **8**, 711–738 (2008).
4. C. Kappel, A. Selle, T. Fricke-Begemann, M. A. Bader, and G. Marowsky, "Giant enhancement of two-photon fluorescence induced by resonant double grating waveguide structures," Appl. Phys. B: Lasers Opt. **79**, 531–534 (2004).
5. G. L. Duveneck, M. A. Bopp, M. Ehrat, M. Haiml, U. Keller, M. A. Bader, G. Marowsky, and S. Soria, "Evanescent-field-induced two-photon fluorescence: excitation of macroscopic areas of planar waveguides," Appl. Phys. B: Lasers Opt. **73**, 869–871 (2001).
6. J. Extermann, L. Bonacina, E. Cuna, C. Kasparian, Y. Mugnier, T. Feurer, and J. P. Wolf, "Nanodoublers as deep imaging markers for multi-photon microscopy," Opt. Express **17**, 15342–15349 (2009).
7. C. L. Hsieh, R. Grange, Y. Pu, and D. Psaltis, "Three-dimensional harmonic holographic microcopy using nanoparticles as probes for cell imaging," Opt. Express **17**, 2880–2891 (2009).
8. A. V. Kachynski, A. N. Kuzmin, M. Nyk, I. Roy, and P. N. Prasad, "Zinc oxide nanocrystals for nonresonant nonlinear optical microscopy in biology and medicine," J. Phys. Chem. C **112**, 10721–10724 (2008).
9. R. Grange, J. W. Choi, C. L. Hsieh, Y. Pu, A. Magrez, R. Smajda, L. Forro, and D. Psaltis, "Lithium niobate nanowires synthesis, optical properties, and manipulation," Appl. Phys. Lett. **95**, 143105 (2009).
10. L. Le Xuan, S. Brasselet, F. Treussart, J. F. Roch, F. Marquier, D. Chauvat, S. Perruchas, C. Tard, and T. Gacoin, "Balanced homodyne detection of second-harmonic generation from isolated subwavelength emitters," Appl. Phys. Lett. **89**, 121118 (2006).

#134892 - $15.00 USD Received 9 Sep 2010; revised 30 Sep 2010; accepted 1 Oct 2010; published 19 Oct 2010

11. J. Extermann, L. Bonacina, F. Courvoisier, D. Kiselev, Y. Mugnier, R. Le Dantec, C. Galez, and J. P. Wolf, "Nano-frog: Frequency resolved optical gating by a nanometric object," Opt. Express **16**, 10405–10411 (2008).
12. P. Wnuk, L. Le Xuan, A. Slablab, C. Tard, S. Perruchas, T. Gacoin, J. F. Roch, D. Chauvat, and C. Radzewicz, "Coherent nonlinear emission from a single ktp nanoparticle with broadband femtosecond pulses," Opt. Express **17**, 4652–4658 (2009).
13. J. Extermann, P. Béjot, L. Bonacina, Y. Mugnier, R. Le Dantec, T. Mazingue, C. Galez, and J. Wolf, "An inexpensive nonlinear medium for intense ultrabroadband pulse characterization," Appl. Phys. B **97**, 537–540 (2009).
14. Y. Shen, J. Swiatkiewicz, J. Winiarz, P. Markowicz, and P. N. Prasad, "Second-harmonic and sum-frequency imaging of organic nanocrystals with photon scanning tunneling microscope," Appl. Phys. Lett. **77**, 2946 (2000).
15. J. Jasny and J. Sepiol, "Single molecules observed by immersion mirror objective. a novel method of finding the orientation of a radiating dipole," Chem. Phys. Lett. **273**, 439–443 (1997).
16. M. Bohmer and J. Enderlein, "Orientation imaging of single molecules by wide-field epifluorescence microscopy," J. Opt. Soc. Am. B **20**, 554–559 (2003).
17. V. Le Floc'h, S. Brasselet, J. F. Roch, and J. Zyss, "Monitoring of orientation in molecular ensembles by polarization sensitive nonlinear microscopy," J. Phys. Chem. B **107**, 12403–12410 (2003).
18. J. I. Dadap, "Optical second-harmonic scattering from cylindrical particles," Phys. Rev. B **78**, 205322 (2008).
19. N. Sandeau, L. Le Xuan, D. Chauvat, C. Zhou, J. F. Roch, and S. Brasselet, "Defocused imaging of second harmonic generation from a single nanocrystal," Opt. Express **15**, 16051–16060 (2007).
20. L. Bonacina, Y. Mugnier, F. Courvoisier, R. Le Dantec, J. Extermann, Y. Lambert, V. Boutou, C. Galez, and J. P. Wolf, "Polar $Fe(IO_3)_3$ nanocrystals as local probes for nonlinear microscopy," Appl. Phys. B: Lasers Opt. **87**, 399–403 (2007).
21. S. W. Liu, H. J. Zhou, A. Ricca, R. Tian, and M. Xiao, "Far-field second-harmonic fingerprint of twinning in single ZnO rods," Phys. Rev. B **77**, 113311 (2008).
22. J. Steyer and W. Almers, "Tracking single secretory granules in live chromaffin cells by evanescent-field fluorescence microscopy," Biophys. J. **76**, 2262–2271 (1999).

1. Introduction

Planar optical waveguides have already been used as a suitable excitation platform in a number of fluorescence analysis applications.[1, 2, 3] They enable highly efficient and selective excitation of fluorescent molecules in close proximity to the waveguide surface by the evanescent field of the guided mode. Typically the waveguide is composed of a single layer of a metal-oxide with high index of refraction. High intensity of the evanescent field is assured by using an appropriate film thickness for single mode operation, usually in the range of 100 - 200 nm. The strong evanescent field of such waveguide modes allows the design of highly sensitive devices and provides the possibility for two-photon fluorescence excitation on comparatively large areas.[4, 5]

Inorganic non-centrosymmetric nanocrystals, often referred to as SHRIMPs (Second Harmonic IMaging Probes), have attracted increasing attention and stimulated a wide series of proposals for their applications in bioimaging [6, 7, 8], micromanipulation [9], and exploitation of their coherent optical response [10, 11, 12] since the appearance of the first studies on their nonlinear optical properties. Due to their sub-wavelength dimensions and related absence of phase-matching constraints [13], there is no spectral limitation for the nonlinear excitation of such nanoparticles. Moreover, in contrast to resonantly excited nanoprobes (such as fluorescent molecules and quantum dots), SHRIMPs are not affected by bleaching nor blinking, the former being one of the principle drawbacks reported in previous waveguide experiments.[5]

In this work we demonstrate non-scanning excitation of the second harmonic (SH) response of several individual SHRIMPs scattered over a large area on a planar waveguide. Although evanescent-field-induced two-photon fluorescence was already demonstrated for homogenous organic layers, this work provides for the first time the evidence of *non-scanning* evanescent excitation of the SH response of nanometric objects. In a similar context, it should be highlighted the experiment realized by the Prasad group on nonlinear excitation of organic nanocrystals with a photon scanning tunneling microscope.[14] Our results are discussed in terms of efficiency and polarization properties. Further information about individual nanoparticles' orientation and coherent emission are derived within the defined image defocusing framework first

#134892 - $15.00 USD Received 9 Sep 2010; revised 30 Sep 2010; accepted 1 Oct 2010; published 19 Oct 2010

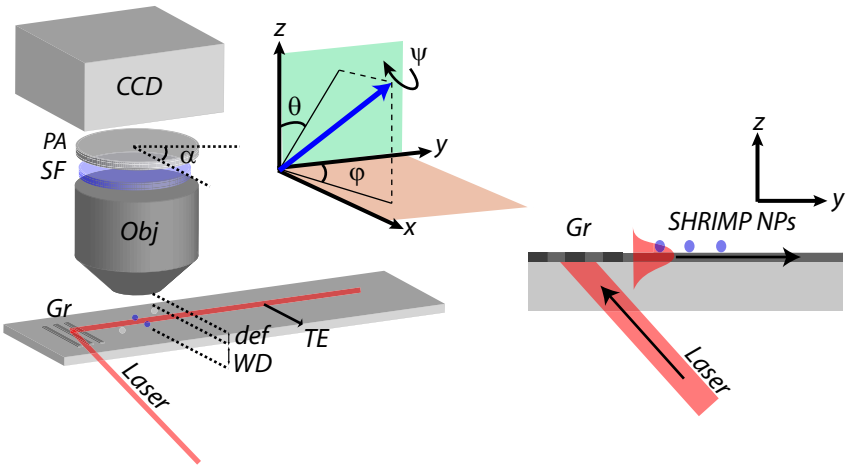

Fig. 1. Experimental setup. Laser radiation is coupled via grating couplers (*Gr*) into the tantalum pentoxide (Ta_2O_5) waveguide which is applied to the surface of a glass substrate. The SH as generated by the nanoparticles on the waveguide is observed by a CCD camera through a microscope objective (*Obj*). *SF*: Spectral Filter. *PA*: Polarization Analyzer. *WD*: Working Distance of the objective. *def*: defocusing parameter. Left: 3D view. Right: side view illustrating the geometry of substrate, waveguide, nanoparticles, incident laser beam and the intensity profile of the guided mode.

developed by Sepiol [15] and later expanded by Enderlein and co-workers.[16]

2. Experimental

The experimental setup is described in Fig. 1. The frequency-doubled output of an ultrashort-pulse Erbium doped fiber laser (Menlo Systems TC1550, central wavelength 780 nm, bandwidth 9 nm, output power 45 mW, repetition rate 80 MHz, pulse duration 150 fs) is coupled with TE polarization under the resonance angle of -48° into a tantalum pentoxide waveguide of thickness 159 nm on a 0.7 mm AF45 glass substrate by a lithographically manufactured grating structure (Balzers Optics, Liechtenstein, grating period $\Lambda = 318$ nm). The guided mode inside the plane waveguide has a lateral extension along the x-direction of 25 μm. TE laser polarization denotes an electric field vector along the *x* axis of the laboratory frame. The coupling efficiency into the waveguide is approximately 20%. Due to the limited spectral acceptance of the grating, the spectral bandwidth of the coupled pulses is reduced to 4 nm, leading to temporal stretching.

Potassium-Titanyl-Phospate (KTiOPO4, KTP) powder (Cristal Laser S.A., Messein - France) was dissolved in demineralized water. A drop (1 μl) of the solution was dispensed onto the waveguide surface at some millimeters from the grating coupler where the solvent evaporated. The histogram of naocrystals size as determined by dynamic light scattering (Malvern Zetasizer NanoZS) is given in Fig. 2(a) inset. The superimposed log-normal fit indicates an average size of 185 nm. The SH radiation emitted by individual SHRIMPs was collected by a 40× magnification objective (Nikon, Plan Fluor ELWD 40x/0.60), spectrally filtered by a multi-photon fluorescence emission filter (Semrock, FF01-750SP, 380-720 nm passband), and detected by a CCD camera (pco.1600, 1200 x 1600 pixels, pixel size 7.4 μm). For polarization analysis, a polarizing plate (Schneider-Kreuznach, AUF-MRC) located in front of the camera sensor was rotated by an angle α, where $\alpha = 0$ corresponds to transmitted *x*-polarization. Defocused

#134892 - $15.00 USD Received 9 Sep 2010; revised 30 Sep 2010; accepted 1 Oct 2010; published 19 Oct 2010

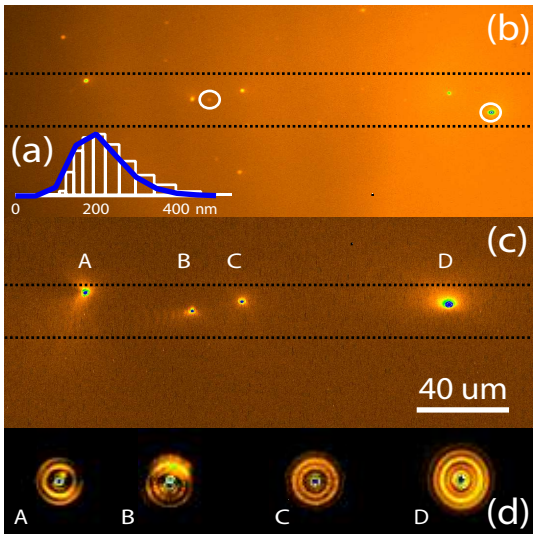

Fig. 2. **(a)** Size distribution by number of the KTP nanocrystals suspension fitted by a log-normal function centered at 185 nm. **(b)** White light image of the scatterers on the waveguide. The dashed lines indicate the extension of the waveguide mode. **(c)** SH image of the same sample region. Note that the particles encircled in the upper plot are not present in the SH image. **(d)** Defocused ($def = 20\ \mu$m) images of the four SH emitting particles of panel (b).

images were acquired by an accurately defined displacement, def, of the detection unit (objective, filter, CCD camera) and thus of the objective's focal plane with respect to the waveguide surface.

3. Imaging

Figure 2(b) presents an image of the nanoparticles spread on the waveguide under white light illumination. The differences in intensity revealed by the particles scattering, originate from the size dispersion of the sample. The lateral extension of the guided mode inside the waveguide is indicated by the two parallel dashed lines. Figure 2(c) represents the same sample region imaged at the SH frequency. The four nanoparticles appearing in this image, labeled $A-D$, are evanescently excited by the laser radiation propagating inside the waveguide. Their positions spatially correlate with those of the nanoparticles observed in Fig. 2(b). Figure 3(a) shows the power dependence of the normalized SH signal generated by these nanoparticles. The response exhibits a clear square dependence shown by the superimposed fit (thick line). This result supports the good spectral selection of the experiment, appreciable also from the extremely high contrast in the SH response of Fig. 2(c). However, one can notice the absence in the SH image of the two nanoparticles encircled in Fig. 2(b) although they are both within the excitation region. The lack of the SH counterparts for these particles cannot be trivially ascribed to a difference in size: this becomes apparent for the right particle, which presents a higher scattering intensity than the average under white light illumination. The missing SH signal of these particles is rather owing to an unfavorable orientation of their crystal axis with respect to the excitation light polarization.

#134892 - $15.00 USD Received 9 Sep 2010; revised 30 Sep 2010; accepted 1 Oct 2010; published 19 Oct 2010

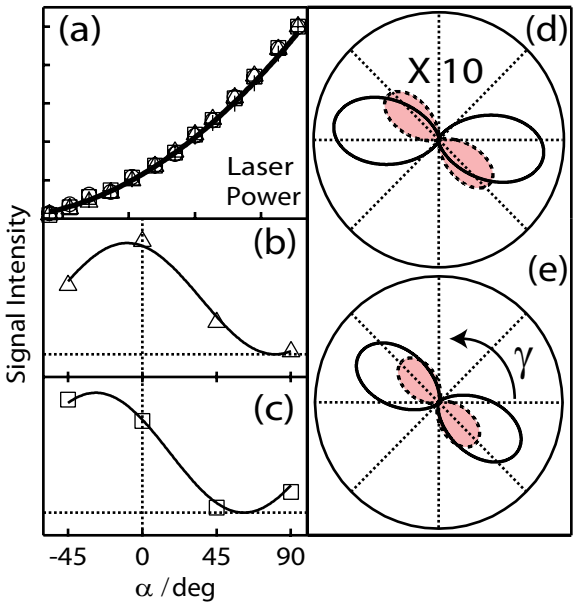

Fig. 3. **(a)** Normalized power dependence of the SH of nanoparticles $A-D$ of Fig. 1(b). **(b)** and **(c)** Polarization dependence of SH emission from particles D (△) and C (□) as a function of the analyzer angle α. **(d)** and **(e)** Calculated intensity dependence of SH emission for particles D and C as a function of excitation light polarization (γ) and analyzer angle (continuous line $\alpha = 0$, dashed line $\alpha = 90°$). Waveguide evanescent excitation corresponds to $\gamma = 0$. Note that the $\alpha = 90°$ response in the upper plot is multiplied by ten for easier inspection.

4. Orientation retrieval

4.1. Polarization analysis

The polarization dependence of the nonlinear response of a nanocrystal can be calculated knowing the nonlinear susceptibility tensor of the material, $\chi^{(2)}$, and the particle orientation with respect to the laser polarization.[17] The induced nonlinear polarization components can be then defined as

$$P_i^{2\omega} = \varepsilon_0 \sum_{jk} \chi_{ijk}^{(2)} E_j^{\omega} E_k^{\omega} \tag{1}$$

Where the $\chi_{ijk}^{(2)}$ tensor is expressed in the laboratory frame and can be derived from the $\chi_{\bar{i}\bar{j}\bar{k}}^{(2)}$ tensor in the crystal frame by

$$\chi_{ijk}^{(2)} = \sum_{\bar{i}\bar{j}\bar{k}} \chi_{\bar{i}\bar{j}\bar{k}}^{(2)} S_{i\bar{i}} S_{j\bar{j}} S_{k\bar{k}} \tag{2}$$

$S_{i\bar{i}}$ being the components of the rotation matrix between the laboratory and crystal axes.[17, 18]

KTP presents an orthorombic crystal structure, where the $\chi_{\bar{z}\bar{z}\bar{z}}^{(2)}$ element is at least four times larger than any other tensorial contribution.[19] The particles highlighted in Fig. 2(b) very likely present an orientation of the crystal frame that leads to a vanishing result for Eq. 1, assuming an electric field vector aligned along x. For particles $A-D$, on the other hand, the SH response is generated quite efficiently.

#134892 - $15.00 USD Received 9 Sep 2010; revised 30 Sep 2010; accepted 1 Oct 2010; published 19 Oct 2010

The polarization of the corresponding $P_i^{2\omega}$ vector is reported in Fig. 3(b) and (c) for particles *D* (△) and *C* (□), respectively. The datapoints represent the SH intensity as a function of the analyzer angle α. Particle *D* (resp. *C*) presents a polarization response peaking at -10° (-28°) and complete signal extinction for 80° (60°), fulfilling the predictions of Malus' law as confirmed by the good agreement with the $\cos^2$ fit (thick line). Starting from Eq. 1, we could simulate the curves in the right panel of Fig. 3, which illustrate the theoretical SH intensity dependence for the two KTP nanocrystals as a function of excitation polarization (γ) and analyzer angle (continuous line $\alpha = 0$, dashed line $\alpha = 90°$). Unlike previous analysis carried out with tight focusing excitation [20, 19], the evanescent wave polarization along *x* ($\gamma = 0$) cannot be simply changed in the present scheme. Therefore the Euler angles $\theta,\ \varphi,\ \psi$ determining the relative orientation of the crystal to the laboratory frame were inferred by matching the intensity of the experimental values obtained for $\alpha = 0$ and $\alpha = 90°$ (Fig. 3(b), (c)) to the corresponding values assumed for $\gamma = 0$ by the simulated traces. Clearly, for a fixed value of γ, the 3-d orientation retrieval remains an under-determined problem. We therefore applied an additional empirical criterion to identify the in-plane crystal orientation φ among the ensemble of possible solutions by setting $\theta, \psi = 90°$ accounting for the experimental bias represented by the most likely detection of intense SH radiation, that for KTP is associated to this orientation. In the next sub-section, we demonstrate that at least the uncertainty on the θ orientation can be lifted by inspecting the symmetry of the defocused emission pattern, on the other hand the determination of ψ given the experimental constrains and the relative magnitudes of KTP $\chi^{(2)}$ tensor remains elusive within this approach. The best correspondence for the in-plane angle of particles *D* and *C* was finally found for $\varphi_D = -10°$ (Fig. 3(d)) and $\varphi_C = -37°$ (Fig. 3(e)).

4.2. Defocused imaging

As just mentioned, the fixed laser polarization of the approach presented above prevents a complete and rigorous orientation retrieval, nevertheless information about the out-of-plane angle θ of the nonlinear dipole can be derived by applying the theoretical model developed by J. Enderlein [16] and already used by Sandeau *et al.* for analyzing the defocused images of SHRIMPs.[19] Figure 2(d) reports the images obtained for particles $A-D$ by displacing the focal plane of the collection objective by def =20 μm from the substrate. One can see that, while particles *C* and *D* present a radial symmetric emission structure with concentric rings of different intensity, particles *A* and *B* are characterized by the presence of weaker intensity regions in their emission patterns (the upper right zone and the bottom half respectively for particles *A* and *B*). In addition, in the series experimental images reported in the first row of Fig. 4, measured by varying the def parameter from 0 to 70 μm, a clear asymmetry is observable for any $def > 0$ in the emission of the lower particle as opposed to the perfectly radial pattern of the upper one.

To understand the origin of these features, we performed a simulation modeling two close lying dipoles, radiating at twice the frequency of the laser ($\lambda = 390$ nm). The defocused images were elaborated taking into full account the imaging set-up, the CCD pixel dimension (7.4 μm), and the waveguide characteristics (n =2.092, 159 nm thickness sustained by a n =1.52 glass substrate). The in-plane and out-of-plane angles of the two dipoles were finally adjusted to obtain the best qualitative agreement with the experimental image. After this procedure, we could ascribe the difference in the symmetry of the two emission patterns principally to a difference in the out-of-plane angles θ. In the case of the upper one, the dipole orientation is parallel to the substrate and to the exciting polarization ($\theta_1 \simeq 90°$), while for the lower one, θ presents a much larger out-of-plane component (($\theta_2 \simeq 33°$)). A similar procedure can be repeated for the particles in Fig. 2(d), ensuring that the out-of-plane angle θ is indeed 90° for particles *C* and *D* as assumed in the previous analysis. It is worth pointing out that all the

#134892 - $15.00 USD Received 9 Sep 2010; revised 30 Sep 2010; accepted 1 Oct 2010; published 19 Oct 2010

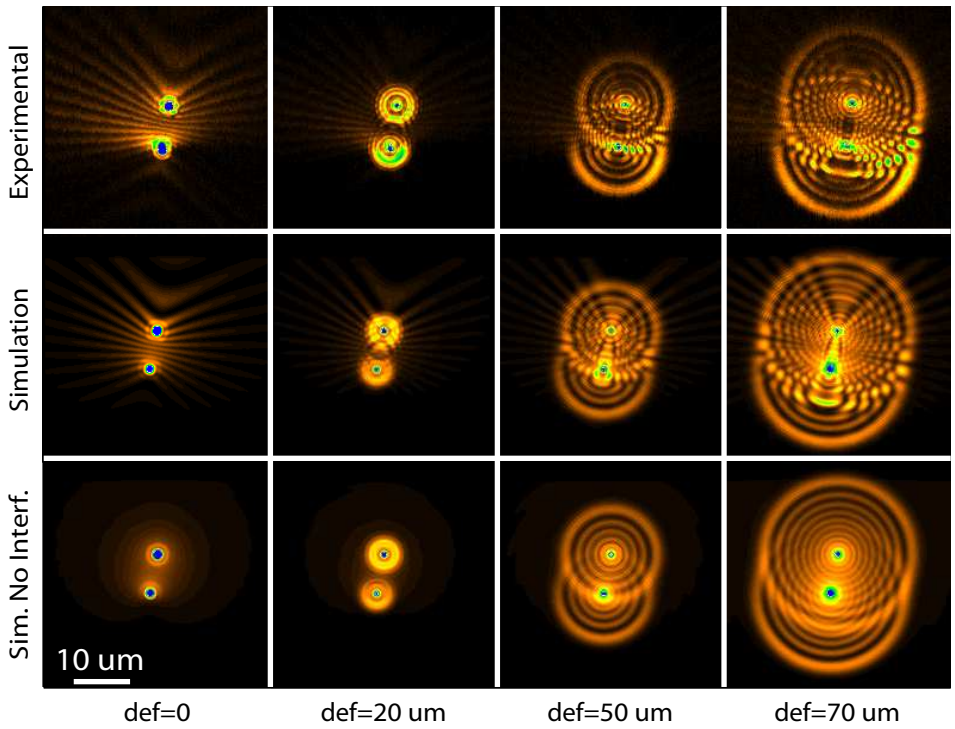

Fig. 4. Experimental (first row) and numerical (second row) images of two adjacent nanoparticles excited by the evanescent field and interfering at the SH frequency for different defocusing parameters: def =0, 20, 50, and 70 μm. The third row contains the corresponding defocused images calculated for the artificial case of no inter-particles interference. The length scale is the same for all plots, the intensity scale are adjusted to facilitate the inspection of interference details but are maintained constant among second and third row for each def value. The resulting out-of-plane orientation of the emitting dipole associated to the upper particle and to the lower particle are $\theta_1 = 90^\circ$ (in-plane) and $\theta_2 = 35^\circ$, respectively.

patterns presented, although not always radial symmetric, systematically present a clear axial symmetry, testifying to the fact that the nonlinearly excited nanocrystals are characterized a single monocrystalline domain.[19]

5. Coherent effects

One very intriguing characteristic emerging from all the images of Fig. 4 is the presence of interference fringes, occurring because of the coherent superposition of the SH emission of the two nanoparticles. Incidentally, analogous structures have been recently observed in the far-field scattering patterns generated by different portions of a micrometric rod.[21] Here interferences appear for small defocusing values as stripes in the region between the two particles and then develop as a dashed motif on the concentric rings of the emission pattern. The simulations capture even the finest details observed in the experimental images. The best agreement was obtained by convoluting the numerical results with a disk of two pixels radius, accounting for the smoothing effect of the not perfectly planar waveguide surface. As an additional proof of the genuine interpretation of the observed patterns as resulting from interferences and to

#134892 - $15.00 USD Received 9 Sep 2010; revised 30 Sep 2010; accepted 1 Oct 2010; published 19 Oct 2010

rule out any alternative explanation based on some critical misalignment of the optical set-up, we provide in the third row of Fig. 4 the corresponding defocused images calculated by artificially switching-off the inter-particles interference term. The false color scales for any given def value are respected in the simulations run with and without this contribution. From the comparison of both approaches with the experimental data, it immediately comes into sight that inter-particle interference plays an essential and unambiguous role in the definition of the observed pattern.

It is worth noting that - unlike the case of harmonic holography, where interferences are created with an external reference beam - we show here interferences originated directly among the nonlinear emissions of two distinct nano-objects for the first time. It should be also pointed out that the clear interference pattern of Fig. 4 is not easily observed. Most of the times, in fact, the latter presents complicated and nonsymmetric structures because of to the presence of several interfering nanoparticles and/or small aggregates. In these cases, the defocused images cannot be easily interpreted and modelled as the coherent superposition of a few, well defined, spatially separated dipoles.

6. Conclusions

This work proves the possibility to employ SHRIMP nanoparticles as molecular probes in experiments based on evanescent excitation, taking full advantage of their photostability and of their non-resonant optical response. High selective evanescent excitation at the substrate surface can be associated to nonlinear transverse resolution for imaging. In principle, for example, SHRIMPs can be used to probe the penetration of the evanescent field more efficiently than fluorescent beads for TIRF experiments.[22] Furthermore, we demonstrated that polarization analysis can be carried out under reasonable assumptions, and the dipole moments associated to individual crystals can be prospectively used as optical probes of the local field [9] in large areas of a waveguide for monitoring, for instance, cells membrane potential. Finally, and for the first time, we observed and numerically modeled the interferences generated from the nonlinear emission of distinct nanometric objects.

Acknowledgments

L. Bonacina acknowledges the financial support of the Swiss Secretary for Research (SER) in the framework of COST MP0604 actions. R. Bäumner and T. Fricke-Begemann gratefully acknowledge financial support by the German Federal Ministry of Economics and Technology (Grant no. 16IN0365). We are grateful to Ronan Le Dantec (SYMME, Université de Savoie) for the DLS measurements.

#134892 - $15.00 USD Received 9 Sep 2010; revised 30 Sep 2010; accepted 1 Oct 2010; published 19 Oct 2010